ENTMOOT: A FRAMEWORK FOR OPTIMIZATION OVER ENSEMBLE TREE MODELS

Alexander Thebelt[*]
Imperial College London,
South Kensington, SW7 2AZ, UK.
alexander.thebelt18@imperial.ac.uk

Jan Kronqvist
Imperial College London,
South Kensington, SW7 2AZ, UK.
j.kronqvist@imperial.ac.uk

Miten Mistry
Imperial College London,
South Kensington, SW7 2AZ, UK.
miten.mistry11@imperial.ac.uk

Robert M. Lee
BASF SE,
Ludwigshafen am Rhein, Germany.
robert-matthew.lee@basf.com

Nathan Sudermann-Merx
BASF SE,
Ludwigshafen am Rhein, Germany.
nathan.sudermann-merx@basf.com

Ruth Misener
Imperial College London,
South Kensington, SW7 2AZ, UK.
r.misener@imperial.ac.uk

May 19, 2021

ABSTRACT

Gradient boosted trees and other regression tree models perform well in a wide range of real-world, industrial applications. These tree models (i) offer insight into important prediction features, (ii) effectively manage sparse data, and (iii) have excellent prediction capabilities. Despite their advantages, they are generally unpopular for decision-making tasks and black-box optimization, which is due to their difficult-to-optimize structure and the lack of a reliable uncertainty measure. ENTMOOT is our new framework for integrating (already trained) tree models into larger optimization problems. The contributions of ENTMOOT include: (i) explicitly introducing a reliable uncertainty measure that is compatible with tree models, (ii) solving the larger optimization problems that incorporate these uncertainty aware tree models, (iii) proving that the solutions are globally optimal, i.e. no better solution exists. In particular, we show how the ENTMOOT approach allows a simple integration of tree models into decision-making and black-box optimization, where it proves as a strong competitor to commonly-used frameworks.

Keywords Bayesian optimization · gradient-boosted trees · deterministic global optimization · black-box optimization

---

[*]Corresponding author

1 Introduction

Recently, Bayesian optimization (BO) has become a popular machine learning-based approach for optimizing black-box functions, with successful applications including hyperparameter tuning of machine learning algorithms [Snoek et al., 2012], design of engineering systems [Forrester et al., 2008, Močkus, 1989] and drug design [Negoescu et al., 2011]. A black-box function $f : \mathbb{R}^n \to \mathbb{R}$ can be evaluated for $\boldsymbol{x} \in \mathbb{R}^n$ but no further information, such as the derivatives, is available. BO proposes sequential function queries $\boldsymbol{x}_{next} \in \mathbb{R}^n$ to iteratively determine the global minimizer $\boldsymbol{x}^*$ of black-box function $f(\boldsymbol{x})$ according to Equ. (1a).

$$\boldsymbol{x}^* \in \operatorname*{argmin}_{\boldsymbol{x} \in \mathbb{R}^n} f(\boldsymbol{x}). \tag{1a}$$

$$\text{s.t. } g(\boldsymbol{x}) = 0, \tag{1b}$$

$$h(\boldsymbol{x}) \leq 0, \tag{1c}$$

The input space $\boldsymbol{x}$ may be subject to explicitly known equality constraints $g(\boldsymbol{x})$ and inequality constraints $h(\boldsymbol{x})$. BO derives $\boldsymbol{x}_{next}$ based on a data-driven surrogate model and an uncertainty measure, quantifying the prediction performance of the surrogate model in different search space areas. Both surrogate model prediction and uncertainty measure are combined in an acquisition function, capturing the *exploitation / exploration*-trade-off. For detailed surrogate modeling and BO reviews, see [Brochu et al., 2009, Frazier, 2018, Frazier and Wang, 2016, Shahriari et al., 2016, Bhosekar and Ierapetritou, 2018, McBride and Sundmacher, 2019]. Besides neural networks [Snoek et al., 2015] and Gaussian processes [Rasmussen and Williams, 2006], tree-based models, e.g. random forests (RFs) [Breiman, 2001] and gradient-boosted regression trees (GBRTs) [Friedman, 2000, 2002], are a popular choice for BO surrogate models. Tree-based models give robust prediction performance and can handle nonlinear and discontinuous system behavior. Combined with fast and sophisticated training libraries [Chen and Guestrin, 2016, Ke et al., 2017], tree models scale well to both large data sets and high-dimensional data. Moreover, tree-based models naturally support categorical features. Shahriari et al. [2016] identify unreliable uncertainty estimates and the lack of gradients when optimizing tree model-based acquisition functions as the main drawbacks, limiting the applicability of tree model-based BO approaches.

ENTMOOT (**EN**semble **T**ree **MO**del **O**ptimization **T**ool) is our novel framework to handle tree-based models in BO applications. We propose an intuitive distance-based measure to provide a reliable uncertainty estimate for tree-based models. ENTMOOT encodes tree-based models, uncertainty estimates and applicable constraints as a mathematical program and uses deterministic optimization to provide the optimal *exploitation / exploration* trade-off. Using mixed-integer optimization, ENTMOOT overcomes the commonly known drawbacks of tree-based models in BO while maintaining their advantages. Moreover, it guarantees feasibility of additional constraints (see: Equ. (1)) up to a given tolerance where $g(\boldsymbol{x})$ and $h(\boldsymbol{x})$ can be of quadratic, i.e. convex and nonconvex quadratic, or linear form. ENTMOOT is easy-to-use as it only introduces a maximum of two additonal hyperparameters for effective uncertainty control. Our numerical study shows the effectiveness of the proposed uncertainty measure and excellent scaling to large

and high-dimensional data sets. ENTMOOT is competitive with other state-of-the-art black-box optimization libraries, deriving better functional values than those found by the competing methods in the majority of runs. ENTMOOT v0.1.4 is open-source and available at: `pypi.org/project/entmoot` and `github.com/cog-imperial/entmoot`.

2 Related work

Various successful applications of BO include hyperparameter tuning, chemical and biomedical engineering, and aerospace design [Frazier, 2018, Shahriari et al., 2016]. BO proposes subsequent black-box queries by optimizing an acquisition function that trades-off exploitation and exploration, derived from prediction mean and uncertainty quantification of the underlying surrogate model. The most popular model architecture in BO, the Gaussian process (GP) [Rasmussen and Williams, 2006], is a predictive model with built-in uncertainty considerations that has been successfully deployed on various occasions. GPs are flexible and have well-calibrated uncertainty quantification making it particularly suitable for BO tasks [Jones, 2001, Osborne et al., 2009]. However, the limitations of GPs for large evaluation budgets and high-dimensional search spaces are well-documented. Different techniques exploit potential additive structures of black-box functions [Gardner et al., 2017, Kandasamy et al., 2015, Wang et al., 2018], or map a high-dimensional input feature space to an unknown low-dimensional one [Garnett et al., 2014, Nayebi et al., 2019, Oh et al., 2018, Wang et al., 2016] to overcome these GP limitations. A recent approach by Eriksson et al. [2019] combines local GP models with problem-dependent trust regions to allow better scalability for large data set in high-dimensional search spaces.

Snoek et al. [2015] use *Bayesian neural networks* to tackle BO for large data sets, achieving a linear scaling with the number of observations rather than the cubic cost of training a GP. This approach uses Bayesian linear regression based on an adaptive set of basis functions which is learned by neural networks. Springenberg et al. [2016] improved the algorithm by introducing a modified Hamiltonian Monte Carlo method . This enhancement offers more robust and scalable behavior compared to standard Bayesian neural networks. We include a comparison against the Springenberg et al. [2016] implementation, i.e. the BOHAMIANN algorithm.

Another prominent alternative to GPs are tree-based ensemble methods, e.g. RFs [Breiman, 2001] and GBRTs [Friedman, 2000, 2002]. Tree-based models consist of decision tree ensembles and scale well to large data sets due to parallelization. Fixed-size subsets of available dimensions define decision nodes of individual trees to provide robust behavior in high-dimensional search spaces. The good predictive performance stems from combing weak tree learners into a tree ensemble. Moreover, tree-based models naturally support various data types, and are preferred over GPs when it comes to categorical and conditional feature spaces. Hutter et al. [2011] first introduced RFs as BO surrogate models. In contrast to GPs, RFs do not natively return model uncertainty at test points required to handle exploration in the acquisition function. Approaches aiming to estimate RF confidence intervals include the *Jackknife* and *Infinitesimal Jackknife* [Wager et al., 2014]. Hutter et al. [2011] propose empirical uncertainty estimates based on predictions of individual trees which have been shown to work well in practice when comparing their algorithm, i.e. SMAC, to

other state-of-the-art BO frameworks. However, Shahriari et al. [2016] point out common settings for which the uncertainty estimate in `SMAC` leads to undesired behavior, i.e. narrow confidence intervals in regions of low data density and uncertainty peaks when individual trees strongly disagree. Moreover, Shahriari et al. [2016] identify the lack of gradients due to the discontinuous and non-differentiable response surface of tree-based models as a main drawback ruling out gradient-based methods to optimize the acquisition function. As a result, most tree-based BO frameworks rely on some sort of sampling approach for optimizing the acquisition function. Another implementation of tree-based models in BO is Scikit-Optimize [The scikit-optimize contributors, 2018] (`SKOPT`) supporting GBRTs as an alternative to RFs. With GBRTs being boosting-type learners, `SKOPT` uses uncertainty estimates derived from quantile regression [Koenker and Hallock, 2001, Meinshausen, 2006]. Multiple GBRT models trained on different quantiles of given observations estimate the prediction uncertainty at test points. `SKOPT` is a well-maintained BO library showing competitive performance against other state-of-the-art BO frameworks. Our numerical tests compare against `SMAC3`, the most up-to-date version of `SMAC`, and both the RF and GBRT variants of `SKOPT`.

Other popular approaches for derivative-free global optimization of black-box functions include evolutionary algorithms based on stochastic optimization, e.g. `CMA-ES`, Nelder-Mead (`NM`) [Nelder and Mead, 1965] and `BFGS` [Zhu et al., 1997]. We include `CMA-ES`, `NM` and `BFGS` as cheap and fast algorithms in our comparison to obtain good baselines for computationally expensive approaches.

Design of experiments [Garud et al., 2017, Hasan et al., 2011] and decision-making using surrogate models is enjoying growing popularity in chemical engineering [Bhosekar and Ierapetritou, 2018]. Some examples use convex region linear estimators [Zhang et al., 2016], algebraic equations [Boukouvala and Floudas, 2017, Wilson and Sahinidis, 2017], artificial neural networks [Henao and Maravelias, 2011, Schweidtmann and Mitsos, 2019, Eason and Cremaschi, 2014, Leperi et al., 2019] and Gaussian processes [Palmer and Realff, 2002, Davis and Ierapetritou, 2007, Caballero and Grossmann, 2008, Olofsson et al., 2019] as surrogate models with some using global strategies for optimization.

3 ENTMOOT for design of experiments

This section derives the problem formulation representing the core of `ENTMOOT`. Section 3.1 introduces a distance measure quantifying model uncertainty for tree-based surrogate models. Section 3.2 presents the full formulation of `ENTMOOT` describing how the exploitation vs. exploration trade-off is realized using tree-based models and the proposed uncertainty measure for tasks related to BO. We introduce formulations for the squared Euclidean and the Manhattan distances as two options to capture model uncertainty.

3.1 Capturing model uncertainty via spatial distance

Tree-based models work well as interpolators, i.e. they have good prediction performance within the data set and especially close to training data. However, they are poor extrapolators with decreasing prediction performance for unexplored regions of the input feature space not covered by training data [Shahriari et al., 2016]. Different methods
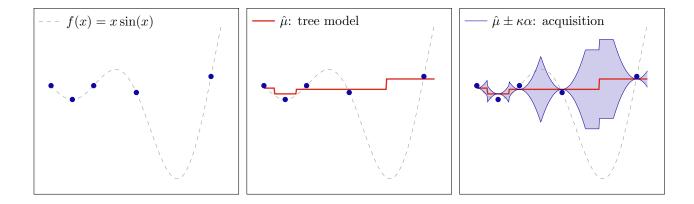
Figure 1: Illustration of ENTMOOT's Equ. (3a) defined exploitation and exploration terms. **(Left)** Plot of the $f(x) = x\sin(x)$ example function and available data points. **(Middle)** GBRT response surface fitted to available data points referring to $\hat{\mu}$ of Equ. (3a). **(Right)** Uncertainty intervals representing $\kappa\alpha$ in Equ. (3a) (lower curve) and Equ. (8a) (upper curve) around the mean prediction of $\hat{\mu}$.

estimating tree-based model uncertainty [Hutter et al., 2011, Meinshausen, 2006, Wager et al., 2014] are successful in practice but may cause unintuitive behavior in BO, like over-exploration or overconfident uncertainty quantification in regions with sparse data. We propose an intuitive estimate α using the distance to the closest point $\boldsymbol{x}_d$ in data set $\mathscr{D}$ to quantify confidence of model predictions:

$$\alpha(\boldsymbol{x}) = \min_{d \in \mathscr{D}} \|\boldsymbol{x} - \boldsymbol{x}_d\|_p. \tag{2}$$

We assume that high values of α indicate large average model errors. Spatial distances are commonly used in training algorithms to quantify the model error and in clustering algorithms, e.g. k-means [Lloyd, 1982], to assess the parity of cluster members. Similarly, kernel-based methods like GPs [Rasmussen and Williams, 2006] typically use a distance metric in the kernel covariance function to quantify similarity of observations and thus, implicitly, prediction uncertainty. ENTMOOT considers both the squared Euclidean and the Manhattan distance metrics, referring to $p = 2$ and $p = 1$ in Equ. (2) . Different distance metrics may be advantageous for different problems. For example, the Manhattan distance is usually preferred over the Euclidean distance in high-dimensional settings [Aggarwal et al., 2001]. The Section 6 provides case studies evaluate how well such a distance-based estimate can capture model-uncertainty of tree-based models. For ENTMOOT, GBRTs are the models of choice.

5

3.2 Optimizing acquisition functions via mixed-integer optimization

The general formulation for BO related tasks, e.g. design of experiments, is:

$$\boldsymbol{x}_{next} \in \underset{(\boldsymbol{x},\boldsymbol{z},\boldsymbol{y},\hat{\mu},\alpha)\in\Omega}{\operatorname{argmin}} \hat{\mu} - \kappa\alpha. \tag{3a}$$

$$\text{s.t.} \;\; \alpha \leq \text{dist}_d(\boldsymbol{x}), \;\; \forall d \in \mathscr{D}, \tag{3b}$$

$$0 \leq \alpha \leq \alpha_{limit}, \tag{3c}$$

where Ω is a set defined by the constraints in Equ. (4) and Equ . (5) and depending on which uncertainty measure is used Equ. (6) or Equ . (7). Variable $\hat{\mu} \in \mathbb{R}$ refers to the tree model prediction capturing how Equ . (3a) exploits the underlying surrogate model to find promising areas in the search space. Variables $\boldsymbol{z} \in \mathbb{R}^{|\mathscr{T}|\times|\mathscr{L}_t|}$ and $\boldsymbol{y} \in \{0,1\}^{n\times|\mathscr{V}_t|}$ mathematically encode the tree model with the index set of trees denoted as $\mathscr{T}$. $\mathscr{L}_t$ and $\mathscr{V}_t$ are dependent on tree $t \in \mathscr{T}$ and denote the index sets of leaves and splits, respectively. Section 3.2.1 gives more details on the encoding of tree models. Variable α handles exploration and quantifies, according to Equ. (2), the degree of uncertainty expected from prediction $\hat{\mu}$. The parameter $\alpha_{limit} \in \mathbb{R}$ provides the upper bound to variable α. Variable $\text{dist}_d(\boldsymbol{x}) \in \mathbb{R}$ encodes the distance to the closest data point and depends on the distance metric used. Both α_{limit} and $\text{dist}_d(\boldsymbol{x})$ are defined in more detail in Sections 3.2.2 and 3.2.3 discussing different distance metrics. In BO, Equ . (3a), or the acquisition function, trades-off exploitation and exploration and its minimizer determines the next black-box query point $\boldsymbol{x}_{next}$. The acquisition function incentivizes high model uncertainties to force the algorithm to explore unknown search space regions. The positive hyperparameter $\kappa \in \mathbb{R}$ balances exploitation and exploration and is a hyperparameter depending on the application. The Equ. (3a) acquisition function, i.e. the lower confidence bound (LCB) [Cox and John, 1997], is available in most BO libraries, e.g. SMAC3 and SKOPT. Figure 1 visualizes the interplay of exploitation and exploration as implemented in ENTMOOT. When combined with tree-based surrogate models Equ. (3a) is commonly minimized in a stochastic fashion, e.g. by random sampling, as the discrete response surface of tree-based models precludes effective use of gradient-based optimization methods [Shahriari et al., 2016]. Consequently, non-optimal solutions to the acquisition function lead to poorly performing query points $\boldsymbol{x}_{next}$. We propose a mixed-integer optimization framework deriving ϵ-global solutions to Equ. (3a), guaranteeing the best trade-off between exploitation and exploration as encapsulated by the acquisition function.

3.2.1 Encoding ensemble tree models

First, we encode the tree-based model with a mixed-integer formulation initially proposed by Mišić [2020]. Mistry et al. [2020] used the same formulation to combine GBRTs together with a continuous regularizer in an optimization problem. Both Mišić [2020] and Mistry et al. [2020], use mathematical programming to determine optimal inputs of tree-based models. We extend this formulation to a full-fledged BO framework with a reliable uncertainty measure, where an acquisition function is subsequently optimized to minimize an unknown black-box function. The following

constraints encode the GBRTs:

$$\hat{\mu} = \sum_{t \in \mathscr{T}} \sum_{l \in \mathscr{L}_t} F_{t,l} z_{t,l}, \tag{4a}$$

$$\sum_{l \in \mathscr{L}_t} z_{t,l} = 1, \qquad \forall t \in \mathscr{T}, \tag{4b}$$

$$\sum_{l \in \text{Left}_{t,s}} z_{t,l} \leq y_{i(s),j(s)}, \qquad \forall t \in \mathscr{T}, \forall s \in \mathscr{V}_t, \tag{4c}$$

$$\sum_{l \in \text{Right}_{t,s}} z_{t,l} \leq 1 - y_{i(s),j(s)}, \qquad \forall t \in \mathscr{T}, \forall s \in \mathscr{V}_t, \tag{4d}$$

$$y_{i,j} \leq y_{i,j+1}, \qquad \forall i \in [n], \forall j \in [m_i - 1], \tag{4e}$$

$$y_{i,j} \in \{0,1\}, \qquad \forall i \in [n], \forall j \in [m_i], \tag{4f}$$

$$z_{t,l} \geq 0, \qquad \forall t \in \mathscr{T}, \forall l \in \mathscr{L}_t. \tag{4g}$$

We define the tree model prediction $\hat{\mu}$ of Equ. (3a) in Equ. (4a) as the sum of all leaf value parameters $F_{t,l}$. The leaves are indexed by $t \in \mathscr{T}$ and $l \in \mathscr{L}_t$, with $\mathscr{T}$ and $\mathscr{L}_t$ defining the set of trees and leaves in every tree t, respectively. Variables $z_{t,l} \in \mathbb{R}$ function as binary switches, determining which leaves are active. Equ . (4b) ensures that only one leaf per tree contributes to the GBRT prediction. Equ . (4c), (4d) and (4e) force all splits $s \in \mathscr{V}_t$, leading to an active leaf, to occur in the correct order. Here $\text{Left}_{t,s}$ and $\text{Right}_{t,s}$ denote the sets of leaf indices $l \in \mathscr{L}_t$ which are left and right of split s in tree t. Binary switches $y_{i(s),j(s)}$ determine which splits are active. Optimizing for variables $\boldsymbol{z}$ and $\boldsymbol{y}$ corresponds to the tree-model contribution in Equ. (3a).

$$x_i \geq v_{i,0} + \sum_{j=1}^{m_i} (v_{i,j} - v_{i,j-1})(1 - y_{i,j}), \qquad \forall i \in [n], \tag{5a}$$

$$x_i \leq v_{i,m_i+1} + \sum_{j=1}^{m_i} (v_{i,j} - v_{i,j-1}) y_{i,j}, \qquad \forall i \in [n], \tag{5b}$$

$$x_i \in \left[v_i^L, v_i^U\right], \qquad \forall i \in [n]. \tag{5c}$$

We introduce linking constraints according to Equ. (5) to assign separate intervals $v_{i,j}$ defined by the tree model splits back to the original continuous search space $\boldsymbol{x} \in \mathbb{R}^n$. Splits are ordered based on their numerical value according to $v_i^L = v_{i,0} < v_{i,1} < ... < v_{i,m_i} < v_{i,m_i+1} = v_i^U$ with v_i^L and v_i^U denoting upper and lower bound, respectively. Figure 2 shows a simple example of how a tree t of tree ensemble $\mathscr{T}$ partitions a two-dimensional feature space according to Equ. (4) and Equ. (5).
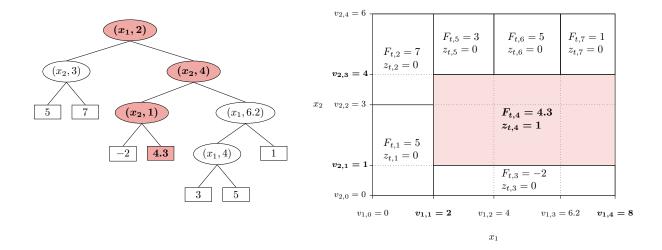
Figure 2: Example evaluation of a decision tree t of a tree ensemble $\mathscr{T}$ for $\boldsymbol{x} = (4.2, 2.8)^T$. **(Left)** Gradient-boosted tree trained for two dimensions. **(Right)** Domain partition according to tree model formulation in Equ. (4) and Equ. (5).

3.2.2 Encoding Euclidean distance squared uncertainty

We derive the exploration term α similar to the Section 3.1 uncertainty measure, considering the Euclidean distance squared to the closest data point of data set $\mathscr{D}$. Constraints (6) complete Equ. (3) by defining $\text{dist}_d(\boldsymbol{x})$:

$$\text{dist}_d(\boldsymbol{x}) \leq \|\boldsymbol{\sigma}_{\mathscr{D},diag}^{-1}(\boldsymbol{x} - \boldsymbol{\mu}_{\mathscr{D}}) - \boldsymbol{x}_d\|_2^2, \qquad \forall d \in \mathscr{D}, \quad (6a)$$

$$\alpha_{limit} = \zeta \, \text{Var}(\boldsymbol{y}_{\mathscr{D}}). \qquad (6b)$$

Equ. (3a) incentivizes larger values for α, i.e. greater distance to the nearest data point, while Equ. (6a) distance constraints to other data points automatically become redundant. As the exploration term α grows quadratically, Equ. (6b) enforces a limit α_{limit} to restrict exploration. The product of hyperparmeter $\zeta \in \mathbb{R}$ and the variance observed in data set target values $\boldsymbol{y}_{\mathscr{D}}$ has shown, in our preliminary studies, to be a good measure. Equ . (6) define our bounded data distance measure. An intuitive interpretation of bounding the data distance is that the model uncertainty is bounded. In other words, setting the hyperparameter ζ incorporates how much more or less variance we expect compared to what is already evident in data set $\mathscr{D}$. Parameters $\boldsymbol{\sigma}_{\mathscr{D},diag} \in \mathbb{R}^{n \times n}$ and $\boldsymbol{\mu}_{\mathscr{D}} \in \mathbb{R}^n$ denote standard deviation and mean of dataset $\mathscr{D}$ and scale variables $\boldsymbol{x}$ as $\boldsymbol{x}_d$ is given in standardized form. The optimization problem defined by objective (3a) and constraints (4), (5) and (6) is a nonconvex mixed-integer quadratic problem.

The nonconvexity arises through the Equ. (3a) negative contribution of variable α in combination with the quadratic term in Equ. (6a). This corresponds to minimizing the blue lower curve on the right-hand side of Fig. 1 which is described by piecewise concave quadratics centered at data points. The resulting optimization problem can be solved to ϵ-global optimality with commercial software, e.g. Gurobi 9 [Gurobi Optimization, 2020].

3.2.3 Encoding Manhattan distance uncertainty

To encode an uncertainty measure using the Manhattan distance metric, we propose a formulation similar to Giloni and Padberg [2002]. The following constraints are added to the optimization problem stated in Equ . (3):

$$\text{dist}_d(\boldsymbol{x}) \leq \sum_{i \in [n]} r_i^{d,+} + r_i^{d,-}, \qquad\qquad \forall d \in \mathscr{D}, \qquad (7a)$$

$$x_i^d - \sigma_i^{-1}(x_i - \mu_i) = r_i^{d,+} - r_i^{d,-}, \qquad\qquad \forall d \in \mathscr{D}, \forall i \in [n]\,, \quad (7b)$$

$$r_i^{d,+} \cdot r_i^{d,-} = 0, \qquad\qquad \forall d \in \mathscr{D}, \forall i \in [n]\,, \quad (7c)$$

$$r_i^{d,+}, r_i^{d,-} \geq 0, \qquad\qquad \forall d \in \mathscr{D}, \forall i \in [n]\,, \quad (7d)$$

$$\alpha_{limit} = \zeta \, \text{Var}(\boldsymbol{y}_{\mathscr{D}}). \qquad\qquad (7e)$$

Depending on the left-hand side of Equ. (7b) being positive or negative, auxiliary variables $r_i^{d,+} \in \mathbb{R}$ or $r_i^{d,-} \in \mathbb{R}$ take the positive distance to the nearest data point in dimension i, respectively. Equ. (7c) forces either $r_i^{d,+}$ or $r_i^{d,-}$ to be zero thereby leading to α taking the value of the Manhattan distance to the closest data point in Equ. (7a) . Parameters σ_i and μ_i correspond to entries (i, i) of $\boldsymbol{\sigma}_{\mathscr{D},diag}$ and i of $\boldsymbol{\mu}_{\mathscr{D}}$, respectively. The optimization problem defined by objective (3a) and constraints (4), (5) and (7) is a mixed-integer linear problem. Bilinear terms in Equ. (7c) are implemented as special ordered sets [Tomlin, 1988] and the problem can be solved to ϵ-global optimality using Gurobi 9.

Compared to the Section 3.2.2 squared Euclidean distance metric, the formulation in Equ. (7) requires a significantly higher number of constraints. The Equ . (6) squared Euclidean distance constraints add one constraint per data point $d \in \mathscr{D}$. In contrast, Equ. (3.2.3) requires one constraint per dimension $i \in [n]$ per data point $d \in \mathscr{D}$. This difference becomes noticeable for high-dimensional problems and translates to longer run times for the Manhattan distance formulation as can be seen in Table 2.

4 ENTMOOT for decision-making under uncertainty

This section builds on Section 3 by deriving a formulation for a related challenge, i.e. decision-making under uncertainty. This considers the case where enough data was gathered to build reliable tree-based models which are then incorporated in wider decision-making problems. A similar formulation considering the previously introduced uncertainty measures is used to incentivize solutions close to training data, i.e. existing knowledge, to minimize the risk of model failure. Moreover, we present algorithmic modifications to allow scalability for handling applications with large data sets and tree models.

To stay close to observed data points in order to minimize the risk of model failure, i.e. predictions with high errors, we consider model uncertainty as a penalty:

$$\boldsymbol{x}_{next} \in \underset{(\boldsymbol{x}, \boldsymbol{z}, \boldsymbol{y}, \hat{\mu}, \alpha) \in \Omega}{\operatorname{argmin}} \hat{\mu} + \kappa\alpha. \tag{8a}$$

$$\text{s.t. } \operatorname{dist}_d(\boldsymbol{x}) \leq \alpha + M(1 - b_d), \quad \forall d \in \mathscr{D}, \tag{8b}$$

$$\sum_{d \in \mathscr{D}} b_d = 1, \tag{8c}$$

$$b_d \in \{0, 1\}, \quad \forall d \in \mathscr{D}, \tag{8d}$$

$$\alpha \geq 0. \tag{8e}$$

When uncertainty contributes as a penalty to the objective function, "big-M" constraints [Nemhauser and Wolsey, 1988] are required to only consider the closest data point. Binary variables $b_d \in \{0, 1\}$ are included into the set of optimization variables and function as a binary switch. When $b_d = 0$, a sufficiently large $M \in \mathbb{R}$ makes Equ. (8b) constraints redundant and thus, deactivates data points that are not the closest ones to $\boldsymbol{x}$. For $b_d = 1$, coefficient M is multiplied by 0 and disappears, causing variable α to take the value of Equ. (8b) left-hand side $\operatorname{dist}_d(\boldsymbol{x})$ which depends on what distance metric is used. Equation (8c) enforces exactly one active data point. For this formulation, a sufficiently large M is:

$$M = \sum_{i \in [n]} \left\| \sigma_i^{-1}(v_i^U - v_i^L) \right\|_p \tag{9}$$

The optimization problem defined by objective (8a) and constraints (4), (5) and (6) is a convex mixed-integer quadratic problem. It corresponds to minimizing the blue upper curve on the right-hand side of Fig. 1 which is described by piecewise convex quadratics centered at data points. When choosing the Equ. (7) Manhattan distance to define $\operatorname{dist}_d(\boldsymbol{x})$ the formulation becomes a mixed-integer linear problem. Both problems can be solved to ϵ-global optimality with commercial software, e.g. Gurobi 9 [Gurobi Optimization, 2020].

4.0.1 Handling large data sets

The Section 4 formulation given in Equ. 8 introduces individual constraints for every data point $d \in \mathscr{D}$. The optimization problem grows quickly with increasing amounts of data. As a solution we propose using a clustering algorithm, e.g.

k-means [Lloyd, 1982], as a pre-processing step. The formulation given in Equ. 8 is replaced by:

$$\boldsymbol{x}_{next} \in \underset{(\boldsymbol{x},\boldsymbol{z},\boldsymbol{y},\hat{\mu},\alpha)\in\Omega}{\operatorname{argmin}} \hat{\mu} + \kappa\alpha. \tag{10a}$$

$$\text{s.t. } \operatorname{dist}_k(\boldsymbol{x}) \le \alpha + M(1 - b_k), \quad \forall k \in \mathscr{K}, \tag{10b}$$

$$\sum_{k\in\mathscr{D}} b_k = 1, \tag{10c}$$

$$b_k \in \{0, 1\}, \tag{10d}$$

$$\alpha \ge 0. \tag{10e}$$

$\mathscr{K}$ denotes the set of cluster centers derived from the clustering. Model uncertainty is then quantified as the distance $\operatorname{dist}_k(\boldsymbol{x})$ to cluster centers instead of data points. For large data sets, this may also lead to more robust behavior of the algorithm as noisy observations will likely be grouped into clusters represented by a single cluster center derived from the mean of all members.

4.0.2 Handling large tree models

When GBRT models become extremely large, i.e. more than 2000 trees with a large number of splits per tree, Gurobi 9 struggles to prove optimality for the large-scale MINLP. To handle these large-scale instances, we propose a more effective bounding strategy [Mistry et al., 2020] in the branch-and-bound algorithm used to solve the underlying mixed-integer problem.

The specifically tailored branch-and-bound approach uses spatial branching over the domain $[\boldsymbol{v}^L, \boldsymbol{v}^U]$. Branch-and-bound characterizes every sub-domain in a minimization problem by a lower objective bound on the best possible solution in the domain. Individual domains are rejected for infeasible subproblems or when their lower bound exceeds the current best feasible solution, i.e. the upper bound. Branch-and-bound thereby aims to avoid explicit enumeration of all possible solutions [Land and Doig, 1960, Morrison et al., 2016]. Like Mistry et al. [2020], we use strong branching to reduce the search space. To compute a new lower bound $\hat{R}^S$ for domain S, ENTMOOT decomposes the Objective (3a) into two parts:

$$\hat{R}^S = b^{\hat{\mu},S} + b^{\alpha,S}, \tag{11}$$

where $b^{\hat{\mu},S}$ and $b^{\alpha,S}$ define the objective lower bounds in domain S for the GBRT model and penalty function, respectively. Computing the tightest objective lower bound for $\hat{\mu}$ in domain S is NP-hard Mišić [2020] and hence, difficult to provide for large GBRT model instances. The approach presented here derives a weaker objective lower bound $b^{\hat{\mu},S}$ by *partition refinement* [Mistry et al., 2020]. We compute $b^{\alpha,S}$ in time linear to the number of clusters multiplied by the number of dimensions, i.e. $\mathcal{O}(|\mathscr{K}| \cdot n)$. This is done by calculating the distance from cluster center $\boldsymbol{x}_k$ to the projection $\boldsymbol{x}'_k$ of the cluster center on box S. The projection $\boldsymbol{x}'_k = (x'_{k,1}, ..., x'_{k,n})^T$ has its elements $x'_{k,i}$
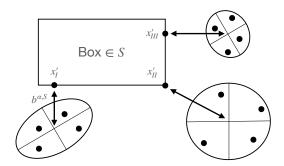
Figure 3: Explicit evaluation of Euclidean distance squared to cluster center projections onto box S for effective computation of $b^{\alpha,S}$.

defined as:

$$
x'_{k,i} = \begin{cases} x_{k,i}, & \text{if } x_{k,i} \in \left[v_i^{L,S}, v_i^{U,S}\right] \\ v_i^{U,S}, & \text{if } x_{k,i} \geq v_i^{U,S} \\ v_i^{L,S}, & \text{if } x_{k,i} \leq v_i^{L,S} \end{cases}, \tag{12}
$$

with $\boldsymbol{v^{L,S}}$ and $\boldsymbol{v^{U,S}}$ denoting upper and lower bounds of box S, respectively. The algorithms picks the minimum of these distances for $b^{\alpha,S}$ or sets it to 0 in case one of the cluster centers is contained in domain S. Figure 3 depicts this procedure. In large data settings the number of clusters can be significantly smaller than the number of data points, i.e. $|\mathcal{K}| << n$. As α increases for regions distant from training data, deriving a weak bound for $\hat{\mu}$ can often reject large domains as the weak lower bound surpasses the current best feasible solution. For domains not rejected based on this penalty condition, $b^{\hat{\mu},S}$ is recomputed to derive tighter bounds for $\hat{\mu}$ in domain S. After every iteration, the best feasible solution and the lowest lower bound converge and ultimately prove global optimality. In practice, the algorithm terminates after reaching a pre-defined optimality gap between best feasible solution and smallest lower bound. From the structure of the problem, we know that pre-defined cluster centers by definition have $\alpha(\boldsymbol{x}_k) = 0$. A good initial feasible solution $\boldsymbol{x}_{feas}$ can therefore be derived by:

$$
\boldsymbol{x}_{feas} = \underset{k \in \mathcal{K}}{\operatorname{argmin}} \; \{\hat{\mu}(\boldsymbol{x}_k)\}. \tag{13}
$$

In Section 6 we present results using a proof-of-concept implementation that shows how the specifically tailored branch-and-bound algorithm with proposed improvements from Section 4.0.2 and Section 4.0.1 leads to faster lower bounding for large tree-model instances.
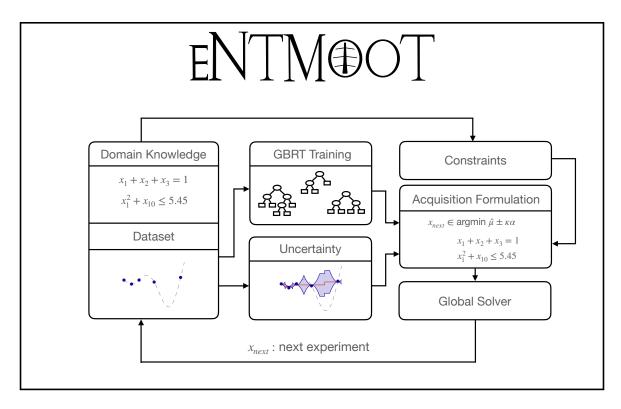
Figure 4: Overview of the `ENTMOOT` toolbox. Available at: `pypi.org/project/entmoot` and `github.com/cog-imperial/entmoot`

5 The ENTMOOT software package

`ENTMOOT`'s functionality is summarized in Figure 5. The tool processes data input provided by the user and hands it over to the global solver to derive x_{next}. The user can provide initial data and application specific constraints regarding features x. The data is used to train GBRT models using LightGBM [Ke et al., 2017] with hyperparameters provided by the user. Moreover, the user specifies which distance metric is used for uncertainty quantification. Both squared Euclidean distance (see: Section 3.2.2) and Manhattan distance (see: Section 3.2.3) are available. Moreover, uncertainty can be quantified with respect to individual data points or cluster centers (See Section 4.0.1 derived from a k-means run.

The acquisition function combines both tree model and model uncertainty. The user can get suggestions x_{next} far from training data as explained in Section 3 or close to existing knowledge according to Section 4. The problem formulation is combined with additional user constraints and given to the global solver. `ENTMOOT` uses the user-specified black-box evaluation budget to terminate the sequential optimization loop. `ENTMOOT` is available on `pypi.org/project/entmoot` and `github.com/cog-imperial/entmoot`.

6 Numerical studies

This section evaluates `ENTMOOT`'s performance on a variety of black-box optimization tasks: a 60D rover navigation problem [Wang et al., 2018], an 80D fermentation optimization [Znad et al., 2004, Elqotbi et al., 2013], a 14D robot

pushing task [Wang et al., 2018] and various multidimensional synthetic benchmark functions. All problems are challenging and commonly used for benchmarking of global black-box optimization tools. We compare against a competitive set of state-of-the-art black-box optimization algorithms from different fields of literature: BOHAMIANN [Springenberg et al., 2016], SMAC3 [Hutter et al., 2011], SKOPT [The scikit-optimize contributors, 2018], CMA-ES [Hansen, 2006], BFGS [Zhu et al., 1997], NELDER-MEAD [Nelder and Mead, 1965]. DUMMY refers to random search and is provided as a weak baseline. For SKOPT, we compare against three different variants which use different underlying surrogate models: SKOPT-GBRT with gradient-boosted trees, SKOPT-RF with random forests and SKOPT-GP with Gaussian processes. For ENTMOOT, we test both metrics for the distance-based uncertainty estimate as proposed in Section 3.2.2 and Section 3.2.3, with ENTMOOT and ENTMOOT-L1 referring to using the squared Euclidean distance and Manhattan distance, respectively. The label ENTMOOT-LARGE refers to using a larger GBRT ensemble, i.e. ensembles using a larger number of tree estimators. While ENTMOOT with a smaller number of trees is easier to optimize due to the smaller resulting optimization model, ENTMOOT-LARGE may have better prediction capabilities as the underlying model is significantly larger. Including both modes in the numerical studies allows us to analyze this trade-off. Hyperparameters for the training of ENTMOOT, ENTMOOT-L1 and ENTMOOT-LARGE are given in Appendix B. Reasonable values for hyperparameters were picked and parameter settings are constant for each mode throughout all tests to allow a fair comparison with other approaches tested. If not indicated otherwise, all algorithms use default settings without hyperparameter tuning for individual runs. Each method is given 50 initial points which are randomly generated from benchmark functions based on random seeds, i.e. the same random seeds are used for every method and are reported in Appendices D.2, D.3 and D.4. Each run has a total budget of 300 black-box evaluation. We report median and confidence intervals by taking the 1st and 3rd quartile of the vector of best objective values found for all random seeds at every iteration. The range between minimum and maximum of the best objective values found is divided by four to determine thresholds for the quartiles. The same random seeds are also used to make optimization methods and noisy black-box functions, i.e. rover navigation and robot push, reproducible. The appendices provide all random states and more details on the individual algorithms and benchmark functions.

This section is divided into four subsections to show: (i) the capabilities of the proposed uncertainty measure independent of the implementation (Section 6.1); (ii) how our proposals contribute to ENTMOOT's competitive performance against other tree-based black-box optimization algorithms (Section 6.2), (iii) how ENTMOOT compares against other state-of-the-art frameworks on commonly-used black-box optimization benchmarks (Section 6.3) and (iv) how algorithmic extensions of ENTMOOT can be used for large-scale applications (Section 6.4).

6.1 Data distance as an effective measure for uncertainty

Section 3.1 proposes using spatial distance as a measure to estimate model uncertainty for tree-based models. While distance metrics are commonly used to describe model errors in training algorithms, there is still a need to analyze how well they capture model uncertainty in tree-based models. With larger distances to training data we expect worse tree
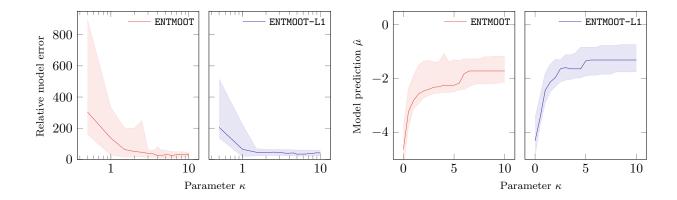
Figure 5: Analysis of uncertainty measure as described in Section 6.1 using proposed optimal points. Hyperparameter κ controls proximity of $\boldsymbol{x}_{next}$ to training data, i.e. high values of κ correspond to closer proximity. **(Left)** Relative error of tree-based models for squared Euclidean distance. **(Left-Middle)** Relative error of tree-based models for Manhattan distance. **(Middle-Right)** Optimal tree model prediction for squared Euclidean distance. **(Right)** Optimal tree model prediction for Manhattan distance.

model prediction performance. We test this hypothesis by changing the objective according to Equ. (8):

$$\boldsymbol{x}_{next} \in \underset{(\boldsymbol{x},\boldsymbol{z},\boldsymbol{y},\hat{\mu},\alpha)\in\Phi}{\operatorname{argmin}} \hat{\mu} + \kappa\alpha, \tag{14}$$

where Φ is a set defined by the constraints in Equ. (4), Equ. (5) and Equ. (8). Changing the sign in Equ. (14) leads to a positive contribution of the distance-based uncertainty measure. This forces ENTMOOT to stay close to training data instead of incentivizing exploration. Adjusting κ in Equ. (14) controls how close the optimal solution is to training data. For the modified optimization model, we expect increasing tree model errors at optimal solutions with decreasing values of κ.

We test on the rover trajectory planning problem which was initially proposed by Wang et al. [2018]. The goal is to propose a fixed number of points in a 2D-plane determining the trajectory of a rover. Different terrain properties influence the reward associated with each proposal. This study uses a smaller 20D variant of the rover trajectory planning problem. Fig. 5 shows the results of the study when adding Equ. (6) or Equ. (7) to set Φ to define the distance metric. As expected, large values for hyperparameter κ lead to less error in the tree model prediction. Moreover, the optimal tree model prediction increases with growing values for κ as the Equ. (14) acquisition function becomes increasingly dominated by the distance measure functioning as a regularizer. The flattening of all curves presented in Fig. 5 corresponds to ENTMOOT converging to the best previously observed data point. Based on this analysis, we can use distance to data points as a measure for uncertainty as it successfully captures prediction performance of tree-based models.

This uncertainty metric is flexible and easily extendable if more information about the black-box function becomes available. For example, if we have information about the input sensitivity, then uncertainty metric terms could be multiplied with pre-determined coefficients to weight the uncertainty contribution of individual features. Similarly, we
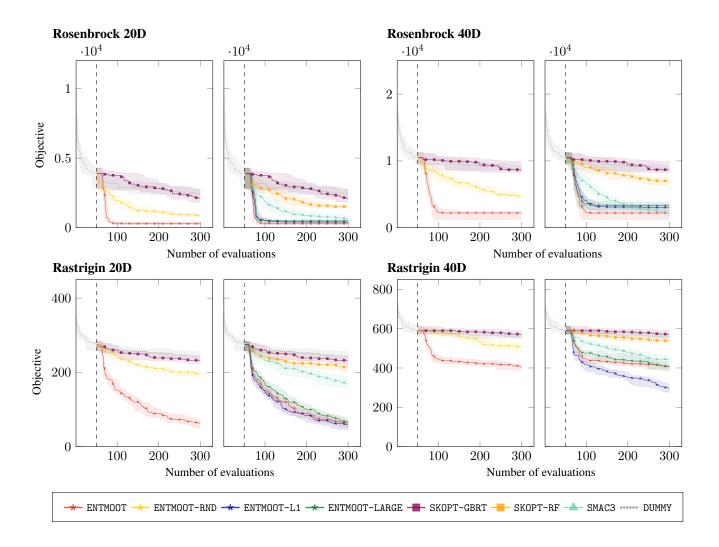
15

Figure 6: Comparison of `ENTMOOT` to other tree model-based black-box optimization frameworks (see: Section 6) for the Rosenbrock and Rastrigin benchmark function. For all black-box functions the left graph emphasizes comparison of uncertainty measure and optimization strategy. The right graph compares `ENTMOOT` against other tree model-based BO tools. Dashed line demarcates initial design.

can incorporate output sensitivity, e.g. assign larger weights to features for which output sensitivity is high. Alternatively, we could use a tree-based uncertainty metric, e.g. as proposed by Mišić [2020].

6.2 Comparison to other tree model-based frameworks

This section tests two features that distinguish `ENTMOOT` from other tree model-based black-box optimization tools: (i) the distance-based measure to capture model uncertainty of tree-based models and (ii) the deterministic global optimization approach that avoids the need for stochastic methods to optimize the acquisition function. Fig. 6 shows the per iteration best objective found by different algorithms on the 20D and 40D Rosenbrock and Rastrigin function. `ENTMOOT-RND` uses the same acquisition function as `ENTMOOT` but random sampling as an optimization strategy to determine new query points for black-box evaluation. This allows a better comparison to `SKOPT-GBRT` which uses
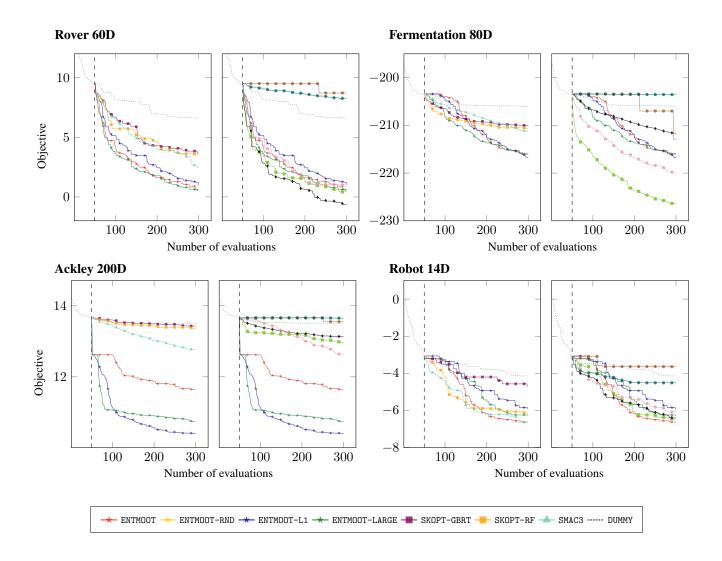
Figure 7: Comparison of `ENTMOOT` to other black-box optimization frameworks (see: Section 6) using various benchmark functions. For all black-box functions the left graph compares `ENTMOOT` against other tree model-based BO tools. The right graph shows how `ENTMOOT` competes against other black-box optimization algorithms. Dashed line demarcates initial design. For graphs that also include confidence intervals we refer to Fig. 10.

the same underlying surrogate model and acquisition function optimization strategy, i.e. exactly the same random samples are used. Purely based on the exploration strategy, `ENTMOOT-RND` can find good solutions to the Rosenbrock function in both dimensional settings and constantly outperforms `SKOPT-GBRT`. Moreover, the default `ENTMOOT` setup, i.e. using deterministic global optimization to optimize the acquisition function, improves over both `SKOPT-GBRT` and `ENTMOOT-RND`. This emphasizes the importance of finding optimal trade-offs of exploitation and exploration when minimizing the acquisition function to determine new query points for black-box evaluations. All `ENTMOOT` variants perform similarly with `ENTMOOT-L1` providing the best objective value for 40D Rastrigin. For Rosenbrock 40D `SMAC3` manages to catch-up towards the end, outperforming both `ENTMOOT-LARGE` and `ENTMOOT-L1` but slightly staying behind the small tree model variant of `ENTMOOT`. Using other synthetic functions, e.g. Sphere, lead to similar results and we refer to the appendices for more results as well as further details of the test setup.

6.3 Comparison to other black-box optimization frameworks

To compare ENTMOOT's performance to other state-of-the-art black-box optimization solvers we test on various difficult instances. The figures compare ENTMOOT to other tree model-based approaches on the left-hand side and ENTMOOT against other black-box optimization frameworks on the right-hand side, i.e. SKOPT-GP, BOHAMIANN, CMA-ES, BFGS and NM. We compare each algorithm's performance on the rover trajectory planning problem [Wang et al., 2018] which is a 60D benchmark instance. Fig. 7 shows how all ENTMOOT variants outperform other tree-based model BO frameworks. In comparison to other black-box optimization frameworks, ENTMOOT is on par with CMA-ES and the Gaussian process based BO tool SKOPT-GP. BOHAMIANN outperforms ENTMOOT with a slightly better black-box objective at the end.

Next, we compare on the fermentation model benchmark which is based on a mechanistic model [Znad et al., 2004, Elqotbi et al., 2013]. This model describes the manufacturing C_P of a chemical product based on a control sequence x consisting of 80 subsequent time steps for which the $k_L a$ value is determined. This value quantifies the efficiency of providing oxygen to the reaction and strongly influences the production. Integrating a system of four differential and one algebraic equation determines the production C_P based on a control sequence x. Here, the well-established SKOPT-GP algorithm based on Gaussian processes takes the lead followed by CMA-ES. However, ENTMOOT significantly outperforms other tree model-based approaches and the neural network approach BOHAMIANN.

In the next study, we evaluate the 200D Ackley function on a domain $[-5, 10]^{200}$ with results given in Fig. 7. All ENTMOOT variants outperform other tree-based model BO frameworks after only a few iterations. ENTMOOT-LARGE and ENTMOOT-L1 perform particularly well on this difficult benchmark problem. Also, in comparison with other black-box optimization tools, ENTMOOT performs best. The 200D Ackley function is notorious for exposing over-exploration in Gaussian process-based BO frameworks as observed by Eriksson et al. [2019] which explains the poor performance of SKOPT-GP.

Finally, we analyze a 14D robot pushing benchmark by Wang et al. [2018] which is considered very challenging for black-box optimization frameworks due to high noise levels in its output and normally requires large evaluation budgets. Fig. 7 shows how every algorithm struggles to consistently provide good solutions leading to large confidence intervals. When analyzing the median, some algorithms consistently perform worse than random sampling, e.g. BFGS, highlighting the difficulty of the benchmark problem. Comparing with other tree-based model frameworks, SMAC3 comes out as the winner, providing a slightly better median solution than ENTMOOT. Compared to other approaches ENTMOOT performs slightly better than BOHAMIANN and SKOPT-GP. For more details on algorithms and benchmark functions, we refer to the appendices. We also provide more details regarding confidence intervals in Fig. 10.

6.4 Large-scale extension

This section provides a proof of concept showing how better objective lower bounding strategies can help handle large-scale tree models. We use the concrete strength data set Yeh [1998] from the UCI machine learning repository Dua and Graff [2017]. The objective is to optimize concrete compressive strength based on ingredient proportions.

We compare Gurobi 9 and `ENTMOOT` runs using advanced optimization strategies from Section 4. Table 1 shows the bound improvements. `ENTMOOT` highly benefits from the warm-starting approach and bounding strategy mentioned in Section 4 and produces better upper and lower bounds after 4 h of runtime. For blank entries in Table 1, `ENTMOOT` has proven ϵ-global optimality already, with a relative optimality gap of 0.01 %. This happens for large penalty hyperparameter values, as large regions can be rejected quickly. In preliminary studies, we found better performance for Gurobi 9 when using the warm-starting strategy. However, for large instances this boost in performance is not sufficient to catch-up with our tailored lower-bounding strategy that exploits the tree structure of the underlying problem. This confirms the findings of Mistry et al. [2020]. While Gurobi 9 is still the best choice for small and moderate instances, i.e. instances that commonly occur in design of experiments, we want to highlight that algorithmic elements exploiting the underlying structure of tree-based models can help when scaling the optimization efforts. Besides Mistry et al. [2020] further improvements for optimizing tree-based models were proposed by Mišić [2020]. For more details regarding the test setup and more results for different κ values, see the appendices.

	ENTMOOT		Gurobi 9.0			ENTMOOT		Gurobi 9.0	
$\kappa = 0.01$	ub	lb	ub	lb	$\kappa = 10$	ub	lb	ub	lb
1 h	-46.8	-50.8	-36.5	-60.5	1 h	-46.8	-50.53	-1.1	-60.5
2 h	-46.8	-49.1	-43.9	-57.3	2 h	-46.8	-48.0	-33.6	-57.7
3 h	-46.8	-48.0	-44.1	-56.6	3 h	-	-	-33.6	-56.7
4 h	-46.8	-47.7	-45.8	-56.5	4 h	-	-	-33.6	-56.5
$\kappa = 0.1$	ub	lb	ub	lb	$\kappa = 100$	ub	lb	ub	lb
1 h	-46.8	-50.8	-40.9	-60.5	1 h	-46.8	-49.7	143.9	-60.5
2 h	-46.8	-49.1	-43.9	-57.4	2 h	-	-	143.9	-57.3
3 h	-46.8	-47.8	-45.0	-56.6	3 h	-	-	0.5	-56.5
4 h	-46.8	-47.6	-45.0	-51.9	4 h	-	-	0.5	-51.8
$\kappa = 1$	ub	lb	ub	lb	$\kappa = 1000$	ub	lb	ub	lb
1 h	-46.8	-50.8	-40.9	-60.5	1 h	-46.8	-49.7	143.9	-60.5
2 h	-46.8	-49.1	-43.9	-57.4	2 h	-	-	143.9	-57.3
3 h	-46.8	-47.8	-45.0	-56.6	3 h	-	-	0.5	-56.5
4 h	-46.8	-47.6	-45.0	-51.9	4 h	-	-	0.5	-51.8

Table 1: Optimization results of `ENTMOOT` and Gurobi 9.0 for a GBT model that is trained on the concrete mixture design dataset. Blank entries refer to convergence of `ENTMOOT` with a relative optimality gap of 0.01 %. Notation is: ub: upper objective bound, i.e. best feasible solution found, lb: lower objective bound, i.e. rigorous underestimator.

7 Conclusion

The success of tools like `SMAC3` and `SKOPT` shows that there is demand for using tree-based surrogate models in global black-box optimization tasks. `ENTMOOT` takes a new approach of handling tree-based models and tackles commonly-known drawbacks of tree-based models in black-box optimization [Shahriari et al., 2016]. By combining an intuitive distance-based uncertainty estimate with a deterministic global optimization strategy, we outperform other tree model-based approaches showing in detail how each of our proposals contributes to `ENTMOOT`'s good performance. On a comprehensive test on real-world complex tasks, `ENTMOOT` is shown to be a strong competitor to other black-box optimization frameworks, either outperforming them or providing competitive results. In most cases `ENTMOOT` finds

excellent solutions after only a few iterations. Moreover, we show how algorithmic improvements can be used to scale the `ENTMOOT` approach to large data sets and tree models.

For the future, we will show how `ENTMOOT`'s support of additional constraints that can be added to the optimization problem helps to include domain knowledge and safety critical requirements, potentially allowing better solutions given less observations. Such constraints can naturally be added to `ENTMOOT`'s deterministic optimization model encoding and solutions guarantee to satisfy the added constraints. Moreover, we hope that the work presented here motivates more efforts in exploring powerful tree-based models in Bayesian optimization settings and applications in chemical engineering.

8 Acknowledgements

A List of Variables, Parameters and Sets

Symbol	Description
f	black-box function
$\boldsymbol{x}$	feature space
n	number of features
$\boldsymbol{x_{next}}$	next proposed point to evaluate
$\boldsymbol{x^*}$	global minimizer of f
$g(\boldsymbol{x})$	equality constraints
$h(\boldsymbol{x})$	inequality constraints
α	uncertainty quantification
κ	acquisition hyperparameter
ζ	exploration hyperparameter
$\hat{\mu}$	mean of tree model
$z_{t,l}$	variable of leaf l in tree t
$y_{i(s),j(s)}$	binary variable of split s in tree model
$F_{t,l}$	value of leaf l in tree t
dist	distance variable
α_{limit}	parameter that limits α
ϵ	optimality gap of MIP solver
v^L	lower bounds of x
v^U	upper bounds of x
v	split interval thresholds
$\sigma_{\mathscr{D},diag}$	diagonal matrix containing standard deviation of data points in $\mathscr{D}$
$\mu_{\mathscr{D}}$	vector containing mean of data points in $\mathscr{D}$
$y_{\mathscr{D}}$	target values in dataset $\mathscr{D}$
$r^{d,+}$	auxiliary variables taking positive contributions of Manhattan distance for data point $d \in \mathscr{D}$
$r^{d,-}$	auxiliary variables taking negative contributions of Manhattan distance for data point $d \in \mathscr{D}$
M	sufficiently large value to allow switching constraints
b	binary variable switch between data points or cluster centers
S	domain S defined by node of branch-and-bound tree
$\hat{R}^S$	lower bound for domain S
$b^{\hat{\mu},S}$	lower bound for tree model in domain S
$b^{\hat{\alpha},S}$	lower bound for tree model uncertainty in domain S
$\boldsymbol{x_{feas}}$	initial feasible solution
C_P	production of chemical product for fermentation benchmark
$k_L a$	quantifies oxygen delivery efficiency for fermentation benchmark

Index	Description
d	data point $d \in \mathscr{D}$
t	trees $t \in \mathscr{T}$
l	leaves $l \in \mathscr{L}_t$
s	splits $s \in \mathscr{V}_t$
i	vector element $i \in [n]$
j	vector element $j \in [m_i]$
k	cluster $k \in \mathscr{K}$

Set	Description
$\mathscr{D}$	dataset
p	order of norm $\|\cdot\|_p$
Ω	constraints defined by tree model and linking constraints
$\mathscr{T}$	index set for trees of tree ensemble
$\mathscr{L}_t$	index set for leaves of tree t
$\mathscr{V}_t$	index set for splits of tree t
$\text{Left}_{t,s}$	index set of leaves left to split s in tree t
$\text{Right}_{t,s}$	index set of leaves right to split s in tree t
$\mathscr{K}$	set of clusters

B ENTMOOT details

In our numerical studies, we use various ENTMOOT settings to show how different features contribute to the performance of the framework. ENTMOOT uses LightGBM [Ke et al., 2017] to train gradient-boosted tree models. The standard ENTMOOT variant as well as ENTMOOT-L1 and ENTMOOT-RND use 400 decision trees per ensemble with an interaction depth of 3. ENTMOOT-LARGE uses an ensemble of 800 decision trees with an interaction depth of 2. Moreover, the minimum number of samples in one leaf is set to 20 and the maximum number of leaves per tree is fixed at 5. All other hyperparameters of LightGBM are left at default values. ENTMOOT-L1 uses the Manhattan distance as an uncertainty estimate which is formally introduced in Section 3.2.3. All other ENTMOOT variants use the squared Euclidean distance

uncertainty measure defined in Section 3.2.2. The uncertainty term in the acquisition function is weighted with κ which is set to a value of 1.96 for all tests, as this is the default value of κ for the SKOPT LCB acquisition function. The uncertainty bound hyperparameter ζ is set to 0.5 for all tests. ENTMOOT-RND uses the same random sampling optimization strategy as SKOPT to minimize the acquisition function. In fact, due to the fixed random seeds in every run, ENTMOOT-RND uses exactly the same sampling points to minimize the acquisition function as SKOPT-GBRT and SKOPT-RF. This allows a direct comparison of the models implemented in both frameworks. All other ENTMOOT variations encode the tree ensemble and the uncertainty estimate as a mathematical model by formulating a MINLP. The model is solved using Gurobi 9 [Gurobi Optimization, 2020], a commercial optimization software. Gurobi 9 is set to a time limit of 2 minutes with most runs finishing at the default relative optimality gap of 0.01 %.

C Other algorithms

This section describes details regarding other algorithms that we compare against ENTMOOT and what specifications were used to run numerical studies. DUMMY randomly samples the search space to find optimal points of benchmark functions. The first 50 points of DUMMY initialize all other algorithms. We define a global random state for every run and use it as the random seed for DUMMY and all non-deterministic algorithms that require a fixed seed for reproducible results.

C.1 BOHAMIANN

The BOHAMIANN framework uses Bayesian neural networks and was first introduced by Springenberg et al. [2016]. We use the RoBo v0.2.0 implementation available at: `https://automl.github.io/RoBO/`. All hyperparameters of BOHAMIANN are left at default values.

C.2 CMA-ES

For comparisons against CMA-ES [Hansen, 2006] we use the cma v3.0.3 implementation available at: `https://pypi.org/project/cma/`. As an initial value x_0, we provided the best point obtained from the initial 50 random values provided by DUMMY. To allow the best possible performance of the framework, we follow recommendations of the user manual and wrap the black-box function to allow standardized inputs. We use the object *CMAEvolutionStrategy* and, based on the scaling, set `sigma0` to 0.5.

C.3 SMAC3

We used the Python implementation SMAC v3 (0.13) [Hutter et al., 2011] by the AutoML group which is available at: `https://github.com/automl/SMAC3`. To get comparable results, we used the SMAC4HPO object which uses random forests as the underlying surrogate model. Given the examples that are tested, we set `run_obj=``quality''` and `deterministic=``true''` as suggested in the user manual. All other hyperparameters are left at default values.

C.4 `SKOPT`

`Scikit-Optimize` (SKOPT) [The scikit-optimize contributors, 2018] is a popular BO library which supports various surrogate models. The numerical studies use the most recent implementation SKOPT v0.8 which is available at: `https://github.com/scikit-optimize/scikit-optimize`. SKOPT-GBRT and SKOPT-RF refer to the `Scikit-Optimize` variants that use GBRTs and RFs as surrogate models, respectively. SKOPT-GP uses GPs as the underlying machine learning model. Besides specifying the surrogate model, all tests were performed with default hyperparameter settings.

C.5 `NELDER-MEAD`, `BFGS`

Both algorithms are implemented as functions in `SciPy` v1.5.3 [Jones et al., 2001] which we used for testing. We lowered the solution tolerances to prevent premature termination, so that both algorithms can make full use of the black-box evaluation budget. For x_0, we provide the best point obtained from the initial 50 random values.

D Numerical studies

D.1 Benchmark functions

This section provides more information for all benchmark functions used. For more detailed information, we refer to the original papers.

D.1.1 Synthetic functions

We use the following synthetic functions [Surjanovic and Bingham, 2020] for testing: Rosenbrock, Rastrigin, Sphere and Styblinski-Tang. We evaluate Rosenbrock on the domain $[-2.048, 2.048]^{dim}$, Rastrigin on $[-5.12, 5.12]^{dim}$, Sphere on $[-5.12, 5.12]^{dim}$ and Styblinski-Tang on $[-5.00, 5.00]^{dim}$. For these functions, we test different dimensionality settings $dim \in \{10, 20, 40\}$. We test Ackley 200D on the domain $[-5.00, 10.00]^{200}$.

D.1.2 Rover trajectory planning

We use a 60D rover trajectory planning problem first proposed by Wang et al. [2018]. The challenge is to fit 30 points on a 2D plane to a B-spline that defines the rover trajectory. The reward is computed based on which terrain the trajectory intersects according to the function: $f(\boldsymbol{x}) = c(\boldsymbol{x}) - 10(\|\boldsymbol{x}_{1,2} - \boldsymbol{x}_s\|_1 + \|\boldsymbol{x}_{59,60} - \boldsymbol{x}_g\|_1) + 5$. More specifically, every collision with rough terrain adds -20 to $c(\boldsymbol{x})$ as a penalty. $\boldsymbol{x}_s$ and $\boldsymbol{x}_g$ are predefined start and end position and a penalty is added if these are not matched. Instead of maximizing the reward, we minimize the negative reward.

D.1.3 Robot pushing

A robot pushing benchmark is used from Wang et al. [2018]. A controller is tuned for two robot hands to move objects to a specified target location. The search space is 14D and the following hyperparameters are tuned: location and

rotation of hands, speed of movement, direction of movement and pushing time. The reward function is: $f(\boldsymbol{x}) = \sum_{i \in \{1,2\}} \|\boldsymbol{x}_{gi} - \boldsymbol{x}_{si}\| - \|\boldsymbol{x}_{gi} - \boldsymbol{x}_{fi}\|$. $\boldsymbol{x}_{si}$, $\boldsymbol{x}_{fi}$ and $\boldsymbol{x}_{gi}$ define initial, final and goal location of objects, respectively. Instead of maximizing the reward we minimize the negative reward.

D.2 Data distance as an effective measure for uncertainty

The Section 6.1 study shows ENTMOOT's uncertainty estimate at work. The purpose is to analyze how well the distance-based concepts defined in Section 3.2.2 and Section 3.2.3 can capture uncertainty in tree model predictions. For analysis, we can change the value of κ and thereby force the optimal solution to be closer or further away from training data.

For this trial, the Gurobi 9 time limit is set to 1 h, with most runs finishing beforehand at the default relative optimality gap of 0.01 %. A set $\kappa \in \{0.5, 1.0, \dots, 10.0\}$ is evaluated and 30 individual runs per method with random states $rnd \in \{101, 102, 103, \dots, 130\}$ define the confidence intervals. We use an initial data set size of 200 randomly generated samples and compute $\boldsymbol{x}_{next}$, i.e. the next black-box evaluation proposal $f(\boldsymbol{x}_{next})$ by ENTMOOT with the modified mathematical model. We calculate the relative model error according to:

$$\epsilon_{\hat{\mu}}(\kappa) = \left\| \frac{\hat{\mu}(\boldsymbol{x}_{next}) - f(\boldsymbol{x}_{next})}{\hat{\mu}(\boldsymbol{x}_{next})} \right\|, \tag{15}$$

with $\hat{\mu}$ defining the tree model prediction. The relative model error $\epsilon_{\hat{\mu}}$ decreases with growing values for κ. Eventually, κ becomes too large and forces $\boldsymbol{x}_{next}$ to take the location of the best available data point. In Fig. 5, this behavior is shown at end of the graph when the relative model error converges asymptotically. With a higher penalty, α dominates the objective in Equ. (14) and tree model predictions at $\boldsymbol{x}_{next}$ become larger and more conservative. Empirically, this shows that the proposed uncertainty estimate works and both measures, introduced in Section 3.2.2 and Section 3.2.3, are good indicators for model uncertainty of tree-based models.

D.3 Comparison to other tree-based model frameworks

This section presents additional results when comparing ENTMOOT's performance to other tree-based model black-box optimization frameworks (see: Section 6.2) for Rosenbrock, Rastrigin, Sphere and Styblinski-Tang benchmark functions given in Fig. 8 and Fig .9. Similar to results presented in Section 6.2, ENTMOOT performs well against other algorithms, especially in high dimensional settings. To compute confidence intervals, we use random states $rnd \in \{101, 102, 103, \dots, 130\}$.

D.4 Comparison to other black-box optimization frameworks

Confidence intervals in the Section 6.3 performance comparison of ENTMOOT with other black-box optimization tools use random states $rnd \in \{101, 102, 103, \dots, 130\}$.
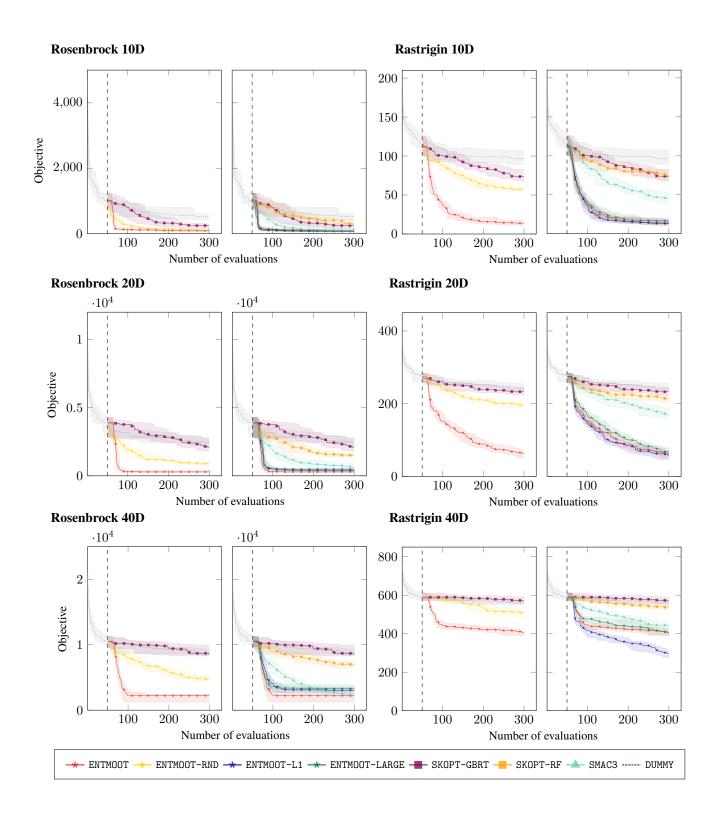
Figure 8: Comparison of `ENTMOOT` to other tree model-based black-box optimization frameworks (see: Section 6) for the Rosenbrock and Rastrigin benchmark functions. For all black-box functions the left graph emphasizes comparison of uncertainty measure and optimization strategy. The right graph compares `ENTMOOT` against other tree model-based BO tools. Dashed line demarcates initial design.
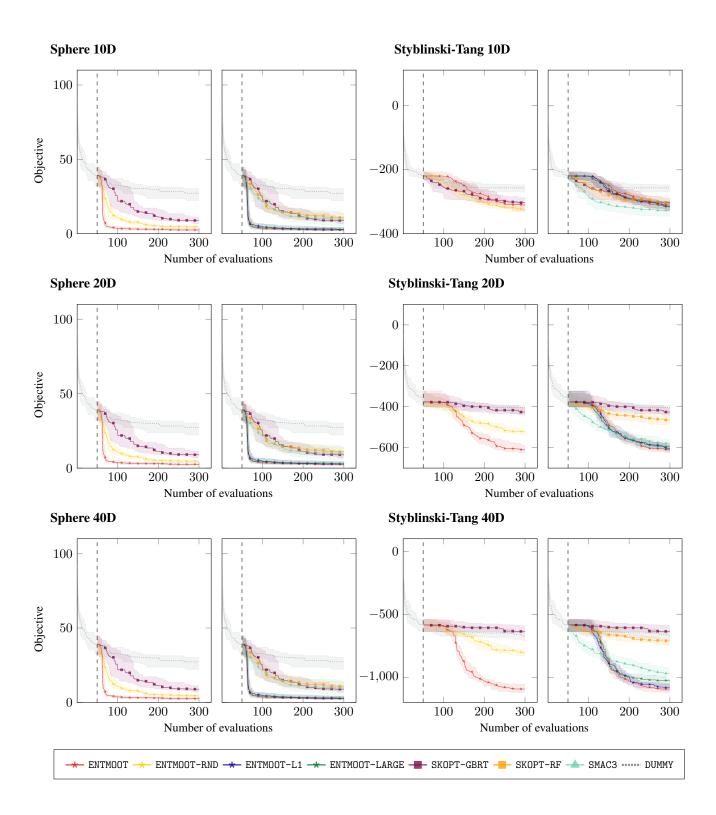
Figure 9: Comparison of ENTMOOT to other tree model-based black-box optimization frameworks (see: Section 6) for the Sphere and Styblinski-Tang benchmark functions. For all black-box functions the left graph emphasizes comparison of uncertainty measure and optimization strategy. The right graph compares ENTMOOT against other tree model-based BO tools. Dashed line demarcates initial design.
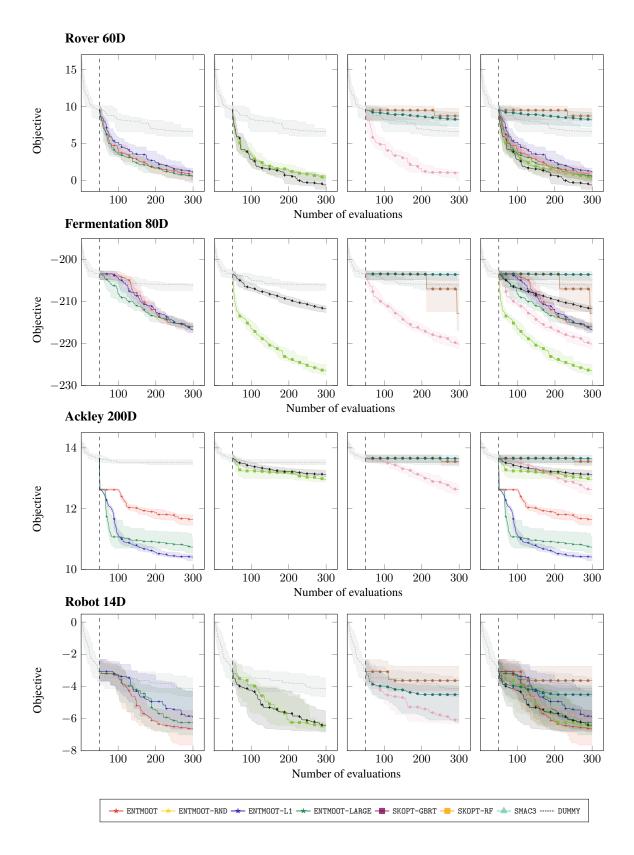
Rover 60D

Fermentation 80D

Ackley 200D

Robot 14D

Figure 10: Comparison of `ENTMOOT` to other black-box optimization frameworks (see: Section 6) using various benchmark functions. Compared to Fig . 7 confidence intervals are shown as well.

D.5   Large-scale extension

Here, we give more details on the large-scale numerical studies performed in Section 6.4. A publicly available dataset [Yeh, 1998] was used which describes the compressive strength of concrete, based on its composition and production procedure defined by features $x \in \mathbb{R}^8$. The dataset is available at the UCI machine learning repository [Dua and Graff, 2017]. We train a large GBT model using 4000 tree estimators, maximum interaction depth of 14, minimum number of samples in leaf of 2, maximum number of leaves of 64 and random state 101. All other hyperparameter settings are left at default values. We do not claim that these hyperparameters make sense for the particular dataset, the point is to show how tailored branch-and-bound algorithms can be used to make ENTMOOT more scalable.

We use 500 clusters for the k-means algorithm, determining the clusters for the cluster distance penalty introduced in Section 4.0.1. Strong branching and partition refinement according to Mistry et al. [2020] is used to handle the large-scale optimization problem. For the strong branching strategy we use a lookahead value of 200, i.e. the algorithm evaluates Equ. (11) $b^{\alpha,S}$ for the next 200 branches that would be explored and removes them if they lead to lower objective bounds above the best feasible solution found so far. The partition refinement is governed by the initial group size of 20 and a fixed bounding time of 120 s per iteration in ENTMOOT and derives Equ. (11) $b^{\hat{\mu},S}$. The underlying mixed-integer linear problem solved during partition refinement is handled by Gurobi 9. These hyperparameter specifications were not optimized and are in line with Mistry et al. [2020], where further details regarding the here mentioned algorithmic concepts can be found. Both the modified ENTMOOT algorithm and Gurobi 9 were tested for hyperparameters $\kappa \in \{0.01, 0.1, 1, 10, 100, 1000\}$, with a fixed time limit of 4 h. Table 1 summarizes the results for all penalty parameter values. Blank entries in Table 1 refer to an early convergence to an ϵ-global optimal solution, given a relative optimality gap of 0.01 %. For the modeling of the mixed-integer programs used in the modified ENTMOOT algorithm we used Pyomo 5.6.7 [Hart et al., 2011].

D.6   Runtime comparison

Table 2 summarizes run times for all algorithm applied to different benchmark problems. The abbreviations *ros*, *ras*, *sph* and *stang* refer to Rosenbrock, Rastrigin, Sphere and Styblinski-Tang benchmark functions, respectively. *ferm*, *rover*, *ackl* and *robot* denote fermentation, rover trajectory planning, Ackley and robot push benchmark problems, respectively. The number in benchmark function names indicates the dimensionality of the problem, e.g. *ackl200* refers to Ackley 200D. Algorithms names *E-GLOB*, *E-RND*, *E-L1* and *E-LARGE* denote ENTMOOT, ENTMOOT-RND, ENTMOOT-L1 and ENTMOOT-LARGE, respectively. SKOPT-GBRT, SKOPT-RF and SKOPT-GP are abbreviated by *S-GBRT*, *S-RF* and *S-GP*. BOHAMIANN is denoted by *BOH*.

Numerical entries in Table 2 indicate $mean(\text{runtime}) \pm standard deviation(\text{runtime})$ derived from all runs presented in the paper. Units are seconds (s), minutes (m) and hours (h). The benchmark studies presented here focus on comparing the quality of solutions derived by individual algorithm. The assumption is that evaluating the black-box function is way more expensive than running an iteration the black-box optimization algorithm. Therefore, ENTMOOT

	E-GLOB	E-RND	E-L1	E-LARGE	SMAC	S-GBRT	S-RF	BOH	S-GP	CMA	BFGS	NM	DUMMY
ros10	5m ± 0	1m ± 0	1.8h ± 0.2	5m ± 1	5m ± 0	38s ± 1	1m ± 0	-	-	-	-	-	4s ± 2
ros20	6m ± 1	1m ± 0	4.9h ± 0.2	8m ± 1	8m ± 0	50s ± 2	1m ± 0	-	-	-	-	-	4s ± 1
ros40	26m ± 10	2m ± 0	4.2h ± 0.5	0.6h ± 0.1	16m ± 1	1m ± 0	2m ± 0	-	-	-	-	-	4s ± 1
ras10	8m ± 1	1m ± 0	4.8h ± 0.3	8m ± 1	4m ± 0	38s ± 1	59s ± 1	-	-	-	-	-	4s ± 2
ras20	2.5h ± 0.8	1m ± 0	7.8h ± 0.1	1.4h ± 0.5	8m ± 0	1m ± 1	1m ± 0	-	-	-	-	-	4s ± 1
ras40	6.4h ± 0.1	2m ± 0	7.7h ± 0.1	6.7h ± 0.1	16m ± 2	1m ± 0	2m ± 0	-	-	-	-	-	5s ± 1
sph10	0.8h ± 0.2	1m ± 0	6.2h ± 0.2	0.6h ± 0.2	5m ± 0	38s ± 1	1m ± 0	-	-	-	-	-	4s ± 2
sph20	5.2h ± 0.2	1m ± 0	7.6h ± 0.1	5.0h ± 0.2	8m ± 0	50s ± 2	1m ± 0	-	-	-	-	-	3s ± 1
sph40	5.9h ± 0.2	2m ± 0	7.7h ± 0.1	6.1h ± 0.1	16m ± 1	1m ± 0	2m ± 0	-	-	-	-	-	4s ± 1
stang10	8m ± 1	1m ± 0	2.9h ± 0.3	10m ± 1	5m ± 0	37s ± 1	1m ± 0	-	-	-	-	-	3s ± 1
stang20	12m ± 2	1m ± 0	6.0h ± 0.1	15m ± 2	8m ± 0	48s ± 1	1m ± 0	-	-	-	-	-	4s ± 2
stang40	1.0h ± 0.3	2m ± 0	5.7h ± 0.2	1.7h ± 0.4	17m ± 1	1m ± 0	2m ± 1	-	-	-	-	-	5s ± 2
ferm80	4.4h ± 1.2	3m ± 0	8.4h ± 0.0	1.5h ± 1.5	0.6h ± 0.0	2m ± 0	3m ± 0	5.8h ± 0.1	1.3h ± 0.2	14s ± 1	17s ± 2	15s ± 2	14s ± 1
rover60	5m ± 1	2m ± 1	9m ± 1	6m ± 1	25m ± 1	2m ± 0	2m ± 0	5.7h ± 0.1	1.3h ± 0.1	5s ± 2	5s ± 1	4s ± 1	4s ± 1
ackl200	7m ± 2	5m ± 0	11m ± 1	7m ± 2	2.1h ± 0.1	5m ± 0	6m ± 0	6.3h ± 0.1	8.0h ± 0.8	4s ± 2	4s ± 1	4s ± 1	7s ± 2
robot14	23m ± 12	1m ± 0	1.3h ± 1.2	18m ± 9	6m ± 0	43s ± 2	1m ± 0	5.5h ± 0.1	29m ± 3	5s ± 2	5s ± 1	4s ± 1	4s ± 1

Table 2: Shows all run times of different tools used for benchmarking. Due to space restrictions we abbreviate both algorithms and benchmark problems.

optimized to find good solutions for benchmark problems but not to minimize its run time. However, when comparing run times `ENTMOOT` performs similar to other sophisticated algorithms like `BOHAMIANN` and `SKOPT-GP`. Also, it is important to emphasize that `ENTMOOT`'s run time can be reduced by lowering the time limit of Gurobi. This may lead to worse black-box function values as the tree-based model may not be optimized to global optimality.

D.7 Computational setup

All numerical results are computed using a Linux machine with 16 GB RAM and an Intel Core i7-7700K @ 4.20 GHz CPU in a `HTCondor` [Thain et al., 2005] setup to allow running multiple experiments in parallel.

References

C. C. Aggarwal, A. Hinneburg, and D. A. Keim. On the Surprising Behavior of Distance Metrics in High Dimensional Spaces. In *Proceedings of the 8th International Conference on Database Theory*, pages 420–434. Springer-Verlag, 2001. ISBN 3540414568.

A. Bhosekar and M. Ierapetritou. Advances in surrogate based modeling, feasibility analysis, and optimization: A review. *Computers & Chemical Engineering*, 108:250–267, 2018.

F. Boukouvala and C. A. Floudas. ARGONAUT: AlgoRithms for Global Optimization of coNstrAined grey-box compUTational problems. *Optimization Letters*, 11(5):895–913, 2017.

L. Breiman. Random Forests. *Machine learning*, 45(1):5–32, 2001.

E. Brochu, M. Cora, and N. de Freitas. A Tutorial on Bayesian Optimization of Expensive Cost Functions, with Application to Active User Modeling and Hierarchical Reinforcement Learning. *ArXiv*, 1012.2599, 2009.

J. A. Caballero and I. E. Grossmann. An algorithm for the use of surrogate models in modular flowsheet optimization. *AIChE journal*, 54(10):2633–2650, 2008.

T. Chen and C. Guestrin. XGBoost: A Scalable Tree Boosting System. In *Proceedings of the 22nd ACM SIGKDD International Conference on Knowledge Discovery and Data Mining*, pages 785–794. Association for Computing Machinery, 2016.

D. D. Cox and S. John. SDO: A Statistical Method for Global Optimization. In *Multidisciplinary Design Optimization: State of the Art*, pages 315–329. Society for Industrial & Applied Mathematics, 1997.

E. Davis and M. Ierapetritou. A kriging method for the solution of nonlinear programs with black-box functions. *AIChE Journal*, 53(8):2001–2012, 2007.

D. Dua and C. Graff. UCI Machine Learning Repository, 2017. URL http://archive.ics.uci.edu/ml.

J. Eason and S. Cremaschi. Adaptive sequential sampling for surrogate model generation with artificial neural networks. *Computers & Chemical Engineering*, 68:220–232, 2014.

M. Elqotbi, S. D. Vlaev, L. Montastruc, and I. Nikov. CFD modelling of two-phase stirred bioreaction systems by segregated solution of the Euler-Euler model. *Computers & Chemical Engineering*, 48:113–120, 2013.

D. Eriksson, M. Poloczek, J. Gardner, R. Turner, and M. Pearce. Scalable Global Optimization via Local Bayesian Optimization. In *Proceedings of the 33rd Conference on Neural Information Processing Systems*, pages 5496–5507, 2019.

A. Forrester, A. Sóbester, and A. Keane. *Engineering Design via Surrogate Modelling: A Practical Guide*. Wiley, 2008.

P. I. Frazier. A Tutorial on Bayesian Optimization. *ArXiv*, 1807.02811, 2018.

P. I. Frazier and J. Wang. *Bayesian optimization for materials design*. Springer, 2016.

J. H. Friedman. Greedy Function Approximation: A Gradient Boosting Machine. *Annals of Statistics*, 29:1189–1232, 2000.

J. H. Friedman. Stochastic gradient boosting. *Computational Statistics & Data Analysis*, 38(4):367–378, 2002.

J. Gardner, C. Guo, K. Weinberger, R. Garnett, and R. Grosse. Discovering and Exploiting Additive Structure for Bayesian Optimization. In *Proceedings of the 20th International Conference on Artificial Intelligence and Statistics*, volume 54, pages 1311–1319, 2017.

R. Garnett, M. A. Osborne, and P. Hennig. Active learning of linear embeddings for Gaussian processes. In *Proceedings of the 30th Conference on Uncertainty in Artificial Intelligence*, pages 230–239, 2014.

S. S. Garud, I. A. Karimi, and M. Kraft. Design of computer experiments: A review. *Computers & Chemical Engineering*, 106:71–95, 2017.

A. Giloni and M. Padberg. Alternative Methods of Linear Regression. *Mathematical and Computer Modeling*, 35:361–374, 2002.

L. Gurobi Optimization. Gurobi Optimizer Reference Manual, 2020. URL `http://www.gurobi.com`.

N. Hansen. *The CMA Evolution Strategy: A Comparing Review*, pages 75–102. Springer Berlin Heidelberg, 2006. ISBN 978-3-540-32494-2.

W. E. Hart, J.-P. Watson, and D. L. Woodruff. Pyomo: modeling and solving mathematical programs in Python. *Mathematical Programming Computation*, 3(3):219–260, 2011.

M. F. Hasan, I. Karimi, S. Farooq, A. Rajendran, and M. Amanullah. Surrogate-based vsa process optimization for post-combustion co2 capture. In *Computer Aided Chemical Engineering*, volume 29, pages 402–406. Elsevier, 2011.

C. A. Henao and C. T. Maravelias. Surrogate-based superstructure optimization framework. *AIChE Journal*, 57(5): 1216–1232, 2011.

F. Hutter, H. H. Hoos, and K. Leyton-Brown. Sequential Model-Based Optimization for General Algorithm Configuration. In *Proceedings of the 5th International Conference on Learning and Intelligent Optimization*, pages 507–523. Springer-Verlag, 2011.

D. R. Jones. A Taxonomy of Global Optimization Methods Based on Response Surfaces. *Journal of Global Optimization*, 21(4):345–383, 2001.

E. Jones, T. Oliphant, and P. Peterson. SciPy: Open Source Scientific Tools for Python, 2001.

K. Kandasamy, J. Schneider, and B. Póczos. High Dimensional Bayesian Optimisation and Bandits via Additive Models. In *Proceedings of the 32nd International Conference on International Conference on Machine Learning*, volume 37, pages 295–304, 2015.

G. Ke, Q. Meng, T. Finley, T. Wang, W. Chen, W. Ma, Q. Ye, and T. Liu. LightGBM: A Highly Efficient Gradient Boosting Decision Tree. In *Proceedings of the 31st International Conference on Neural Information Processing Systems*, pages 3149–3157. Curran Associates Inc., 2017.

R. Koenker and K. Hallock. Quantile Regression. *Journal of Economic Perspectives*, 15(4):143–156, 2001.

A. H. Land and A. G. Doig. An automatic method of solving discrete programming problems. *Econometrica*, 28: 497–520, 1960.

K. T. Leperi, D. Yancy-Caballero, R. Q. Snurr, and F. You. 110th anniversary: Surrogate models based on artificial neural networks to simulate and optimize pressure swing adsorption cycles for co2 capture. *Industrial & Engineering Chemistry Research*, 58(39):18241–18252, 2019.

S. P. Lloyd. Least Squares Quantization in PCM. *IEEE Transactions on Information Theory*, 28(2):129–137, 1982.

K. McBride and K. Sundmacher. Overview of surrogate modeling in chemical process engineering. *Chemie Ingenieur Technik*, 91(3):228–239, 2019.

N. Meinshausen. Quantile Regression Forests. *Journal of Machine Learning Research*, 7:983–999, 2006.

V. V. Mišić. Optimization of Tree Ensembles. *Operations Research*, 2020.

M. Mistry, D. Letsios, G. Krennrich, R. M. Lee, and R. Misener. Mixed-Integer Convex Nonlinear Optimization with Gradient-Boosted Trees Embedded. *INFORMS Journal on Computing*, 2020.

D. R. Morrison, S. H. Jacobson, J. J. Sauppe, and E. C. Sewell. Branch-and-bound algorithms: A survey of recent advances in searching, branching, and pruning. *Discrete Optimization*, 19:79–102, 2016.

J. Močkus. *Bayesian Approach to Global Optimization: Theory and Applications*. Kluwer Academic Publishers, 1989.

A. Nayebi, A. Munteanu, and M. Poloczek. A Framework for Bayesian Optimization in Embedded Subspaces. In *Proceedings of the 36th International Conference on Machine Learning*, pages 4752–4761, 2019.

D. M. Negoescu, P. I. Frazier, and W. Powell. The knowledge gradient algorithm for sequencing experiments in drug discovery. *INFORMS Journal on Computing*, 1(23):46–363, 2011.

J. A. Nelder and R. Mead. A Simplex Method for Function Minimization. *The Computer Journal*, 7:308–313, 1965.

G. Nemhauser and L. Wolsey. *Integer and Combinatorial Optimization*. John Wiley & Sons, Inc., 1988.

C. Oh, E. Gavves, and M. Welling. BOCK : Bayesian Optimization with Cylindrical Kernels. In *Proceedings of the 35th International Conference on Machine Learning*, volume 80, pages 3865–3874, 2018.

S. Olofsson, M. Mehrian, R. Calandra, L. Geris, M. P. Deisenroth, and R. Misener. Bayesian Multiobjective Optimisation With Mixed Analytical and Black-Box Functions: Application to Tissue Engineering. *IEEE Transactions on Biomedical Engineering*, 66(3):727–739, 2019.

M. A. Osborne, R. Garnett, and S. J. Roberts. Gaussian Processes for Global Optimization. In *Learning and Intelligent Optimization*, 2009.

K. Palmer and M. Realff. Optimization and Validation of Steady-State Flowsheet Simulation Metamodels. *Chemical Engineering Research and Design*, 80(7):773–782, 2002.

C. E. Rasmussen and C. K. I. Williams. *Gaussian Processes for Machine Learning*. The MIT Press, 2006.

A. M. Schweidtmann and A. Mitsos. Deterministic Global Optimization with Artificial Neural Networks Embedded. *Journal of Optimization Theory and Applications*, 180(3):925–948, 2019. doi: 10.1007/s10957-018-1396-0.

B. Shahriari, K. Swersky, Z. Wang, R. P. Adams, and N. de Freitas. Taking the Human Out of the Loop: A Review of Bayesian Optimization. *Proceedings of the IEEE*, 104(1):148–175, 2016.

J. Snoek, H. Larochelle, and R. P. Adams. Practical Bayesian Optimization of Machine Learning Algorithms. In *Proceedings of the 25th International Conference on Neural Information Processing Systems*, volume 2, pages 2951–2959. Curran Associates Inc., 2012.

J. Snoek, O. Rippel, K. Swersky, R. Kiros, N. Satish, N. Sundaram, M. M. A. Patwary, Prabhat, and R. P. Adams. Scalable Bayesian Optimization Using Deep Neural Networks. In *Proceedings of the 32nd International Conference on International Conference on Machine Learning*, volume 37, pages 2171–2180, 2015.

J. T. Springenberg, A. Klein, S. Falkner, and F. Hutter. Bayesian Optimization with Robust Bayesian Neural Networks. In *Advances in Neural Information Processing Systems 29*, pages 4141–4149. Curran Associates Inc., 2016. ISBN 9781510838819.

S. Surjanovic and D. Bingham. Virtual Library of Simulation Experiments: Test Functions and Datasets, 2020. URL `http://www.sfu.ca/~ssurjano`.

D. Thain, T. Tannenbaum, and M. Livny. Distributed computing in practice: the Condor experience. *Concurrency - Practice and Experience*, 17(2-4):323–356, 2005.

The scikit-optimize contributors. scikit-optimize/scikit-optimize: v0.5.2, 2018. URL `https://doi.org/10.5281/zenodo.1207017`.

J. A. Tomlin. Special ordered sets and an application to gas supply operations planning. *Mathematical Programming*, 42(1):69–84, 1988.

S. Wager, T. Hastie, and B. Efron. Confidence Intervals for Random Forests: The Jackknife and the Infinitesimal Jackknife. *Journal of Machine Learning Research*, 15:1625–1651, 2014.

Z. Wang, F. Hutter, M. Zoghi, D. Matheson, and N. de Freitas. Bayesian optimization in a billion dimensions via random embeddings. *Journal of Artificial Intelligence Research*, 55(1):361–387, 2016.

Z. Wang, C. Gehring, P. Kohli, and S. Jegelka. Batched Large-scale Bayesian Optimization in High-dimensional Spaces. In *International Conference on Artificial Intelligence and Statistics*, pages 745–754, 2018.

Z. T. Wilson and N. V. Sahinidis. The ALAMO approach to machine learning. *Computers & Chemical Engineering*, 106:785–795, nov 2017.

I. C. Yeh. Modeling of strength of high-performance concrete using artificial neural networks. *Cement and Concrete Research*, 28(12):1797–1808, 1998.

Q. Zhang, I. E. Grossmann, A. Sundaramoorthy, and J. M. Pinto. Data-driven construction of convex region surrogate models. *optimization and Engineering*, 17(2):289–332, 2016.

C. Zhu, R. H. Byrd, P. Lu, and J. Nocedal. Algorithm 778: L-BFGS-B: Fortran subroutines for large-scale bound-constrained optimization. *ACM Transactions on Mathematical Software*, 23:550–560, 1997.

H. Znad, M. Blažej, V. Báleš, and J. Markoš. A kinetic model for gluconic acid production by Aspergillus niger. *Chemical Papers*, 58(1):23, 2004.